Molecular Therapy
Original Article

Nanoparticle Delivery of RIG-I Agonist Enables Effective and Safe Adjuvant Therapy in Pancreatic Cancer

Manisit Das,[1] Limei Shen,[1] Qi Liu,[1,2] Tyler J. Goodwin,[1,3] and Leaf Huang[1,2]

[1]Division of Pharmacoengineering and Molecular Pharmaceutics, Center for Nanotechnology in Drug Delivery, Eshelman School of Pharmacy, University of North Carolina at Chapel Hill, Chapel Hill, NC 27599, USA; [2]UNC & NCSU Joint Department of Biomedical Engineering, University of North Carolina at Chapel Hill, Chapel Hill, NC 27599, USA

Local immunomodulation can be a promising strategy to augment the efficacy and decrease off-target toxicities associated with cancer treatment. Pancreatic cancer is resistant to immunotherapies due to the immunosuppressive tumor microenvironment. Herein, we investigated a therapeutic approach involving delivery of a short interfering double-stranded RNA (dsRNA), specific to *Bcl2*, with 5′ triphosphate ends, by lipid calcium phosphate nanoparticles, in an orthotopic allograft KPC model of pancreatic cancer. Retinoic acid-inducible gene I (RIG-I)-like receptors can bind to 5′ triphosphate dsRNA (ppp dsRNA), a pathogen-associated molecular pattern, producing type I interferon, while *Bcl2* silencing can drive apoptosis of cancer cells. Our approach demonstrated a robust enrichment of tumor tissue with therapeutic nanoparticles and enabled a significant tumor growth inhibition, prolonging median overall survival. Nanoparticles encapsulating dual-therapeutic ppp dsRNA allowed strong induction in levels of pro-inflammatory Th1 cytokines, further increasing proportions of $CD8^+$ T cells over regulatory T cells, M1 over M2 macrophages, and decreased levels of immunosuppressive B regulatory and plasma cells in the tumor microenvironment. Thus, these results provide a new immunotherapy approach for pancreatic cancer.

INTRODUCTION

Resistance to conventional and standard regimens of adjuvant chemotherapy makes pancreatic ductal adenocarcinoma (PDAC) one of the deadliest malignancies, with 5-year survival rates less than 10%.[1,2] Immunotherapy is an attractive strategy, due to relatively high specificity and long-term efficacy. However, dense fibroblast and stroma-rich tumor structure hinder therapeutic delivery to the tumor. Further, an immunosuppressive microenvironment guided by tumor-infiltrating immune cells including tumor-associated macrophages (TAMs), regulatory T cells (Tregs), and myeloid-derived suppressor cells (MDSCs) neutralizes therapeutic benefit.[3] Thus, a robust strategy against pancreatic cancer should be able to satisfy the dual objective of direct cancer cell killing as well as successful modulation of the immunosuppressive tumor microenvironment.

Cells are equipped with pattern recognition receptors (PRRs) that can recognize pathogen-associated molecular patterns (PAMPs) during microbial infection.[4] Retinoic acid-inducible gene I (RIG-I)-like receptors (RLRs), a class of cytosolic PRRs, can detect double-stranded and single-stranded RNA, including RNAs with a triphosphate group at the 5′ ends.[5,6] RLRs trigger caspase activation and recruitment domains (CARDs), which interact with mitochondrial antiviral-signaling protein, triggering transcription factors resulting in induction of type I interferons (IFN-α/β) and other pro-inflammatory cytokine secretion downstream.[7]

Lately, there is an increased interest in harnessing the potential of RLR activation to antitumor immunity. Ellermeier et al.[8] incorporated a triphosphate group at the 5′ end of a short interfering RNA (siRNA) and combined gene silencing with pro-inflammatory RIG-I activation. In a murine pancreatic cancer model, the treatment induced tumor cell apoptosis and augmented levels of type I (IFN-α/β) and type II (IFN-γ) IFNs, skewing T helper (Th) cell response[9] from anti-inflammatory to pro-inflammatory subtype. Poeck et al.[10] also exploited a similar strategy in treating melanoma by using a dual-therapeutic ligand both targeting RIG-I and silencing anti-apoptotic Bcl-2. *Bcl2* gene silencing was reported as a promising therapeutic strategy in multiple cancer models.[11,12]

Previous studies exploited high-dose nucleic acid delivery and repeated administration, resulting in systemic immune activation manifested by elevated levels of pro-inflammatory IFN-γ and tumor necrosis factor alpha (TNF-α) in serum after treatment with 5′ triphosphate double-stranded RNA (ppp dsRNA).[8,10] In human patients, systemic immune activation may contribute to severe immune-related adverse events (irAEs). Thus, multiple clinical trials

Received 29 March 2018; accepted 11 November 2018;
https://doi.org/10.1016/j.ymthe.2018.11.012.

[3]Present address: Precision BioSciences, Inc., Durham, NC, USA.

Correspondence: Leaf Huang, Division of Pharmacoengineering and Molecular Pharmaceutics, Center for Nanotechnology in Drug Delivery, Eshelman School of Pharmacy, University of North Carolina at Chapel Hill, Chapel Hill, NC 27599, USA.
E-mail: leafh@email.unc.edu

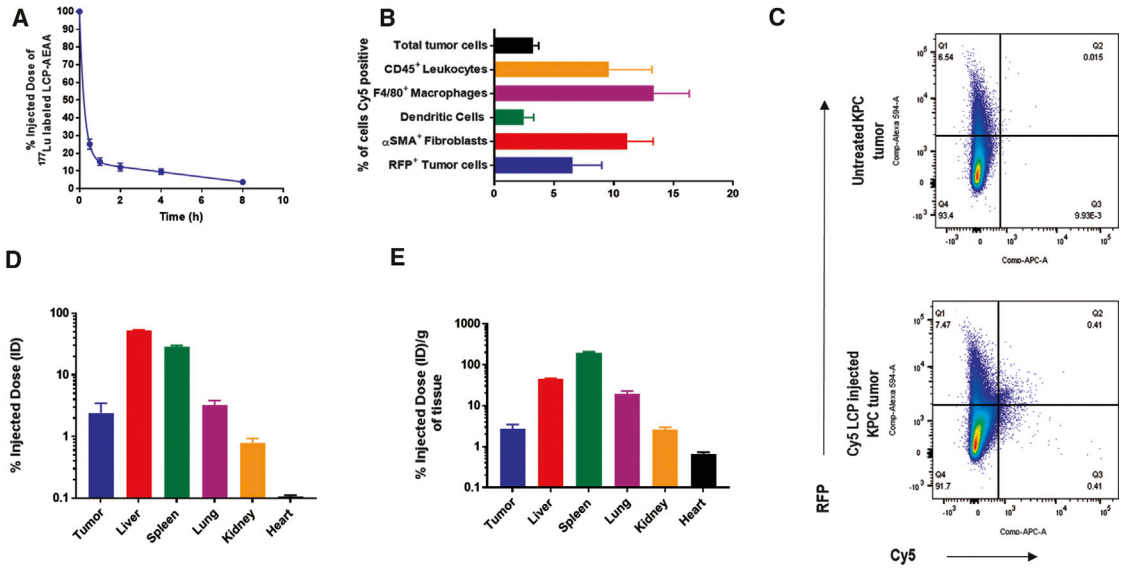

Figure 1. Characterization of LCP-AEAA Nanoparticles and *In Vivo* Uptake on KPC Tumor

(A) Pharmacokinetics of intravenously (i.v.) injected LCP-AEAA by ^{177}Lu (n = 3) radiolabeling. (B and C) LCP-AEAA nanoparticles with Cy5-labeled oligo encapsulated in the core were i.v. injected into mice bearing KPC-RFP/Luc (KPC cell line transfected with mCherry red fluorescent protein and firefly luciferase) tumor (n = 3). The Cy5-positive population within different cell types in the tumor is shown. (B) Mice were sacrificed 18 hr post-injection, and the % of Cy5-positive cells in each cell population was quantified by flow cytometry. (C) Representative flow cytometry graphs for RFP-positive Cy5-positive cells are shown. (D and E) Biodistribution of ^{177}Lu LCP-AEAA nanoparticles 24 hr post-intravenous administration (n = 3). Percent of injected dose (D) and percent of injected dose per gram of tissue (E) are reported. Data are presented as mean ± SEM.

have exploited local delivery of PAMPs by intra-tumoral injection[13] to reduce the systemic toxicity.

Lipid calcium phosphate (LCP) nanoparticles (NPs) had been established as a versatile non-viral gene delivery tool, allowing encapsulation of a broad range of phosphorylated biologics.[14] Herein, we have investigated the efficacy of an LCP NP formulation (LCP-AEAA), targeted with aminoethyl anisamide (AEAA) encapsulating dual-therapeutic ppp dsRNA as a systemic adjuvant against PDAC. KPC, a genetically engineered mouse model with mutations in proto-oncogene K-Ras and tumor-suppressor p53 mutations, is widely considered to be a clinically relevant model of PDAC.[15–17] For ease of monitoring, an allograft-orthotopic model was established using a primary cell line generated from KPC mice. We hypothesize that NP-mediated delivery of ppp dsRNA will elicit a robust primary tumor regression and significant progression-free survival of the host in this PDAC model without any significant irAEs. We tested the hypothesis in this immunocompetent orthotopic model and observed a significant tumor regression with ppp dsRNA LCP-AEAA NPs after uptake in the tumor and subsequent modulation of the immune microenvironment, combined with *Bcl2* gene silencing. No significant toxicities were observed after therapy.

RESULTS

Design and Characterization of ppp dsRNA LCP-AEAA NPs to Allow Specific Delivery to KPC Tumor

For the current study, LCP-AEAA NPs were encapsulated with ppp dsRNA (Figure S1A). Dynamic light scattering (DLS) revealed a major peak of the LCP-AEAA NP size around 32 nm with a subsequent higher peak at ~255 nm because of excess 1,2-dioleoyl-3-trimethylammonium-propane chloride salt (DOTAP) and cholesterol-forming liposomes,[18] resulting in a final Z-average hydrodynamic size of 184 nm (Figure S1B).

LCP-AEAA NPs demonstrated a rapid distribution phase with a half-life of ~22 min (Figure 1A). Cy5-oligo-labeled LCP-AEAA NPs were exploited to analyze the cellular distribution in the KPC orthotopic allograft tumor. About 3.3% ± 0.4% of all cells in the tumor took up the NPs, after a single administration via tail vein (Figures 1B and 1C). Biodistribution studies at 24 hr post-administration (Figures 1D and 1E) recover about 2%–3% injected dose (ID) from the tumor.

AEAA was chemically conjugated to 1,2-distearoryl-sn-glycero-3-phosphoethanolamine-N-[methoxy(polyethyleneglycol-2000)] ammonium salt (DSPE-PEG) to design the molecule (DSPE-PEG-AEAA) used for targeting sigma receptor (Figure S1A). We validated sigma receptor expression on KPC tumor by immunofluorescence (IF) (Figure S2A). Finally, biodistribution data at 18 hr post-administration of Cy5-oligo-labeled LCP NPs show a significant difference in NP uptake (Figure S2B) in KPC tumor when targeted (LCP-AEAA) with AEAA (1.7% ± 0.4%) versus no (LCP) active targeting (0.5% ± 0.0%).

Overall, our results show that systemically administered LCP-AEAA encapsulating ppp dsRNA can be successfully delivered and modestly taken up by different cellular populations in the tumor, and uptake is further augmented by sigma receptor targeting.

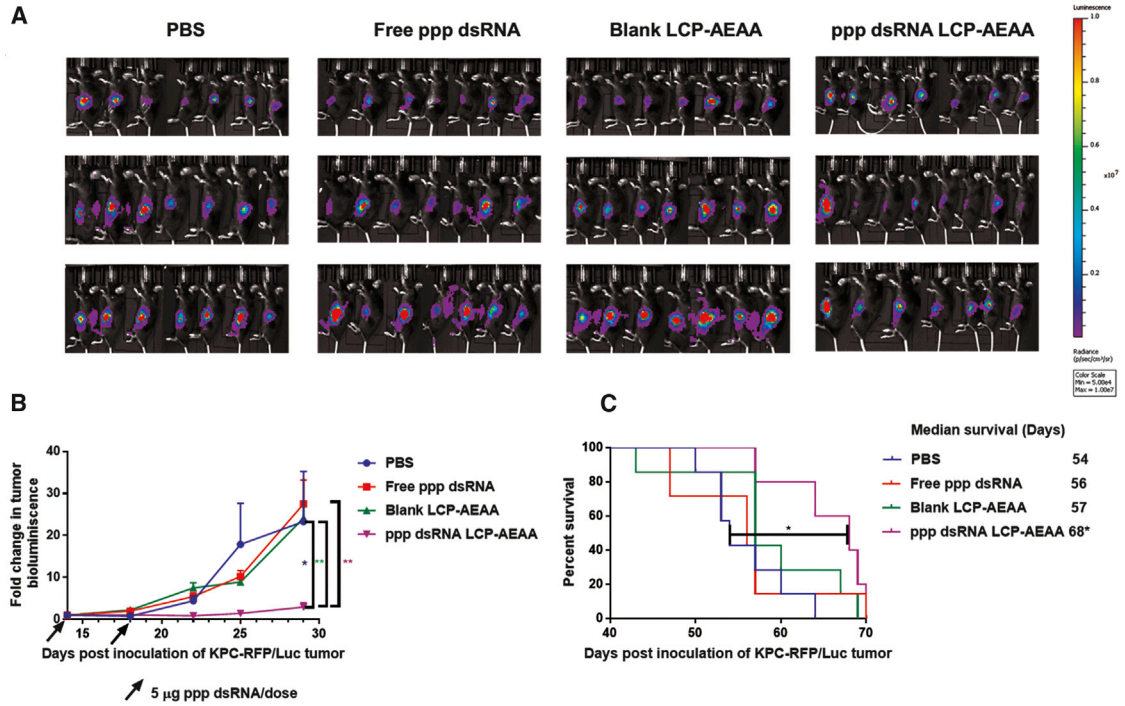

Figure 2. Tumor Growth Inhibition and Survival

(A) *In vivo* bioluminescence images of orthotopic allograft KPC-RFP/Luc tumor after treatment with PBS, free ppp dsRNA, blank LCP-AEAA, and ppp dsRNA LCP-AEAA. Bioluminescence images from representative days post-tumor inoculation are reported. (B) Tumor inhibition curve of KPC-RFP/Luc model. Mice were intravenously (i.v.) injected with different therapeutic interventions post-tumor inoculation (10^6 KPC-RFP/Luc cells/mice). Mice in free ppp dsRNA and ppp dsRNA LCP-AEAA groups received 5 μg of ppp dsRNA per dose. Data are shown as mean ± SEM (n = 7–10). *$p < 0.05$; **$p < 0.01$. (C) Survival of KPC-RFP/Luc tumor-bearing mice across treatment groups (n = 5–7). ppp dsRNA LCP-AEAA significantly prolongs survival with respect to the PBS group.

Monotherapy with LCP-AEAA Encapsulating ppp dsRNA Induced Effective Antitumor Response in Desmoplastic Murine Models of Pancreatic Cancer and Melanoma

C57BL/6 mice bearing KPC-RFP (red fluorescent protein)/Luc (luciferase) tumors were administered with two subsequent doses of RIG-I agonist ppp dsRNA, encapsulated in LCP-AEAA NPs. Free ppp dsRNAs without any delivery vector, PBS, and empty LCP NPs were used as controls. Bioluminescence imaging (BLI) was used to monitor tumor growth, as presented in Figure 2A and quantitatively expressed by a tumor growth curve (Figure 2B), which suggested a significant decrease in tumor progression when treated with LCP-AEAA containing ppp dsRNA. Further, when we investigated the overall survival of the tumor-bearing mice, we observed a significant enhancement (Figure 2C) in median survival (68 days post-inoculation) over untreated control (54 days) ($p < 0.05$). Targeting sigma receptor using AEAA further improves the therapeutic response in terms of tumor regression when compared with untargeted LCPs, as shown in Figure S2C. Masson's trichrome stains of the KPC tumors after different treatments were presented in Figure S4.

To further explore whether we can attain a similar therapeutic response in other desmoplastic cancer models, we investigated the efficacy of the ppp dsRNA LCP-AEAA NPs in a BRAF mutant BPD6 ($BRAF^{V600E}$, $PTEN^{-/-}$, syngeneic with C57BL/6) melanoma model.[19] A significant growth inhibition (Figure S5) was observed with ppp dsRNA LCP-AEAA (498 ± 43 mm^3) over untreated PBS control (1,085 ± 71 mm^3). Free ppp dsRNA (758 ± 66 mm^3) manifested a partial, weaker growth inhibition.

RIG-I Agonist Modulates KPC Tumor Microenvironment by Altering Levels of Tumor-Infiltrating Immune Cells and Cytokine Signaling

Our tumor infiltrate analyses showed that, when treated with ppp dsRNA, the T cell infiltrate was skewed toward $CD8^+$ effector T cells. The CD8/CD4 ratio increased by ~3.5-fold (Figure 3A) in the ppp dsRNA LCP-AEAA group over PBS. The trend holds true if we compare the ratio of $CD8^+$ T cells and Tregs. An ~4-fold increase in CD8/Tregs ratio was observed in the ppp dsRNA LCP-AEAA group over PBS (Figure 4C). Overall, T cells play an important role in the therapeutic effect of ppp dsRNA LCP-AEAA, and the antitumor efficacy was lost when CD8 and CD4 T cells were depleted *in vivo* using antibodies (Figures 4A and 4B).

RIG-I agonist ppp dsRNA treatment significantly decreased immunosuppressive $CD206^+$ $F4/80^+$ M2 macrophages, and the macrophage polarization shifted to a pro-inflammatory $CD206^-$ $F4/80^+$ M1 phenotype. The mean M1 over M2 ratio was 7.7 in the ppp

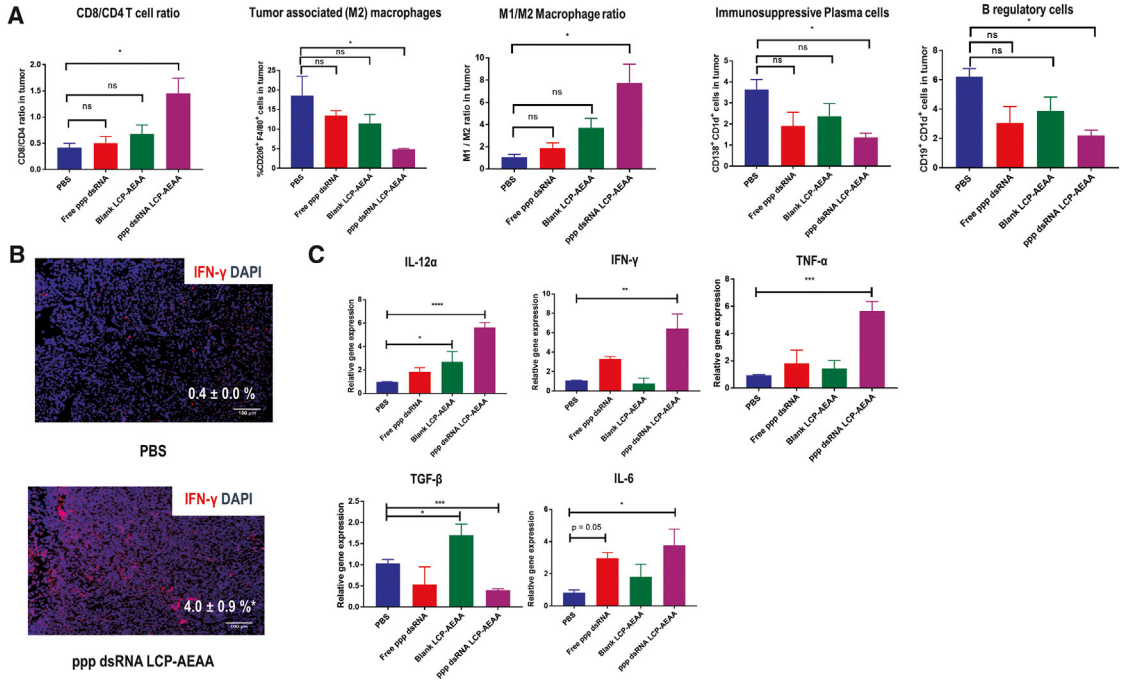

Figure 3. Changes of Tumor-Infiltrating Immune Cells and Cytokines in Response to Therapy

(A) Post-treatment, KPC-RFP/Luc tumor-bearing mice from intervention groups (n = 3) were randomly sacrificed (day 22). Tumor tissues were harvested, and single-cell suspensions were stained and analyzed by flow cytometry. (B) Immunofluorescence microscopy shows upregulation of IFN-γ in tumor, when treated with ppp dsRNA LCP-AEAA. Scale bar, 100 μm. DAPI stains blue for nuclei, and IFN-γ stains red. (C) Tumor tissues were harvested, and total RNA was isolated followed by cDNA synthesis. The resultant cDNA samples were utilized for gene expression analysis using qPCR. The statistical analyses were performed by comparison with the control PBS group. All data show mean ± SEM (n = 3). *$p < 0.05$; **$p < 0.01$; ***$p < 0.001$; ****$p < 0.0001$.

dsRNA LCP-AEAA group compared with 1.1 in the PBS group, indicating a strong polarization toward a proinflammatory M1 phenotype with treatment. We also observed a significant decrease in $CD19^+$ $CD1d^+$ regulatory B cells (Bregs) and $CD138^+$ $CD1d^+$ immunosuppressive cells in the ppp dsRNA LCP-AEAA group over PBS control (Figure 3A). Overall, we observe a noticeable reduction in some major populations of immunosuppressive cells favoring enhancement in proportions of $CD8^+$ T cells and a dramatic shift toward a proinflammatory M1 macrophage phenotype.

To further determine whether cytokine changes drive the alterations in tumor infiltrate populations, we investigated changes in cytokine levels in the tumor microenvironment. IF staining demonstrated a marked expression of proinflammatory IFN-γ within the tumor region in the ppp dsRNA LCP-AEAA-treated group (Figure 3B). We further validated this observation by qPCR, and significant enhancement in levels of the Th1 cytokines IFN-γ, interleukin (IL)-12α, and TNF-α were observed with ppp dsRNA LCP-AEAA treatment (Figure 3C). A significant decrease in immunosuppressive Th2 cytokine transforming growth factor-β1 (TGF-β1) was also determined in the ppp dsRNA LCP-AEAA group over the untreated control. However, the ppp dsRNA LCP-AEAA group also demonstrated a significant elevation in IL-6 levels.

To determine early-onset immune alteration, we investigated cytokine changes in KPC-RFP/Luc tumors 18 hr after administration of ppp dsRNA (Figure 5A). A significant enhancement in IFN-γ and a significant attenuation in IL-10 were observed after treatment with ppp dsRNA LCP-AEAA. Next, we investigated the plasmacytoid dendritic cells (pDCs), a subset of the DCs known for producing type I IFNs, upon activation by PRRs.[20] The percentage of pDCs producing IFN-α was significantly upregulated in the ppp dsRNA LCP-AEAA arm (48.6% ± 12.4%) over the PBS arm (17.7% ± 1.4%).

Bcl2 Gene Silencing Contributes to the Antitumor Efficacy of ppp dsRNA LCP-AEAA

We observed a significant enhancement in the percentage of apoptotic cells in the ppp dsRNA LCP-AEAA group (12.3% ± 3.2%) over PBS (0.6% ± 0.1%) by quantification of terminal deoxynucleotidyl transferase (TdT) dUTP nick-end labeling (TUNEL) assay (Figure 5B). Because *Bcl2* siRNA function was incorporated in the design of the ppp dsRNA, we investigated the gene expression of *Bcl2* in the different groups following treatment. A significant reduction in the expression of the anti-apoptotic *Bcl2* gene was observed in the ppp dsRNA LCP-AEAA group (Figure 5C). Finally, to determine the contribution of Bcl2 silencing to the therapeutic success, we compared the tumor regression effect of ppp dsRNA with a control double-stranded siRNA against *Bcl2* without the 5′ triphosphate

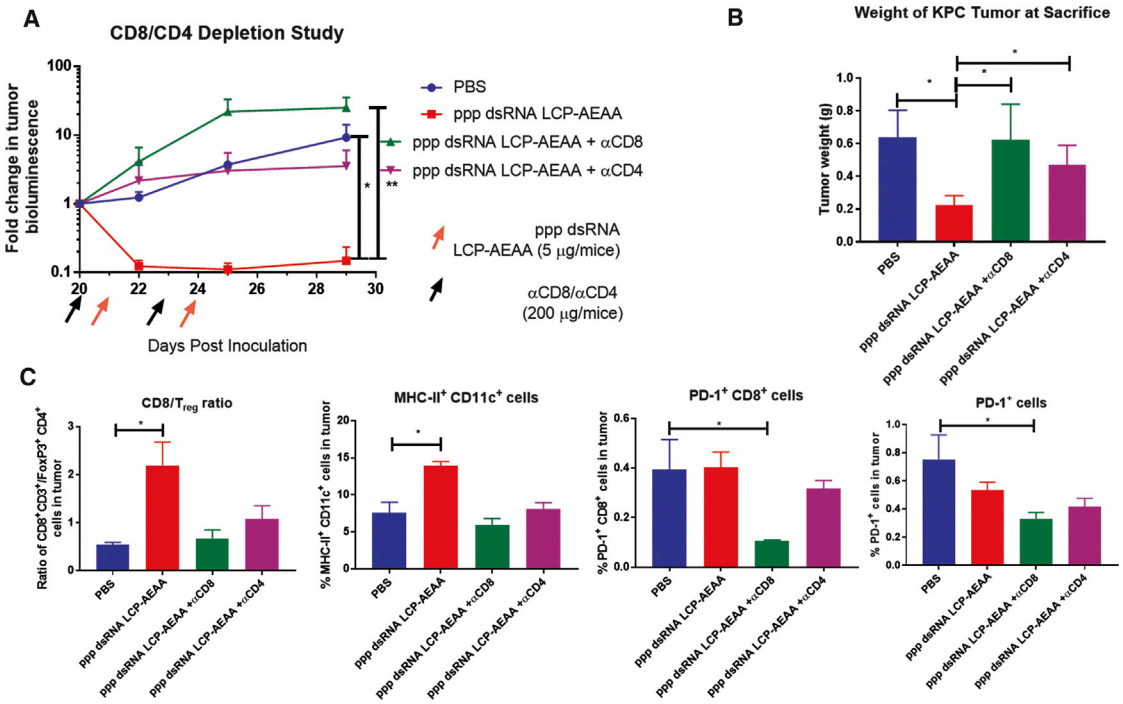

Figure 4. Effect of T Cell Depletion on ppp dsRNA LCP-AEAA Therapy

(A) KPC-RFP/Luc tumor-bearing mice were treated with ppp dsRNA LCP-AEAA intravenously. Mice were pre-treated with anti-CD8 and anti-CD4 antibodies intraperitoneally 1 day before administration of the ppp dsRNA LCP-AEAA nanoparticles. Tumor growth was monitored, and fold change was quantified by bioluminescence imaging. (B) Mice were sacrificed on day 29 after inoculation at the end of the study, and pancreatic tumor weights were compared between the treatment groups (n = 3–4). (C) Post-treatment, KPC-RFP/Luc tumor-bearing mice from intervention groups (n = 3) were sacrificed (day 29). Tumor tissues were harvested, and single-cell suspensions were stained and analyzed by flow cytometry.

group (dsRNA). dsRNA LCP was shown to be only partially effective compared with ppp dsRNA LCP-AEAA, suggesting that RIG-I activation and Bcl2 gene silencing together enable the antitumor efficacy of ppp dsRNA LCP-AEAA.

ppp dsRNA LCP-AEAA Is Non-toxic and Does Not Induce Systemic Immunomodulation

To investigate systemic immunomodulation, we conducted flow cytometry analysis to look at different immune cell populations in the spleen and lymph nodes (Figure 6). We did not observe any significant changes in any major leukocyte population (Figure 6B), and further no pro-inflammatory signatures like skewness toward $CD8^+$ over $CD4^+$ T cells, increase in the numbers of activated DCs (major histocompatibility complex class II^+ [MHC-II^+] $CD11c^+$ cells), or decrease in Breg subsets were observed in spleen samples of KPC tumor-bearing mice 4 days after ppp dsRNA LCP-AEAA administration (Figure 6A). Additional toxicity studies were conducted at 16 hr post-administration of ppp dsRNA LCP-AEAA and other appropriate controls, using naive syngeneic C57BL/6 mice bearing no tumor to determine immune cell activation in the spleen and the lymph nodes. Increase in $CD3^+$ T cells with ppp dsRNA LCP-AEAA in the lymph nodes (Figures S6A and S6B) was the only significant change noted. Representative liver histopathology from the different groups was shown after the toxicity study (Figure S6C).

We further conducted toxicological evaluations to determine whether ppp dsRNA LCP-AEAA can induce any noticeable irAEs. Serum analysis revealed no significant changes in the kidney (creatinine and blood urea nitrogen [BUN]) and liver (aspartate transaminase [AST]) functions (Figure 5B). Further, for the whole blood cell counts, all parameters remained within the normal range and did not manifest a significant deviation from untreated control groups.

DISCUSSION

Downstream RIG-I-mediated pro-inflammatory signaling is dependent on direct binding of ppp dsRNA to cytosolic innate immune sensor protein RIG-I.[21] Hence efficient delivery of an RIG-I agonist for potent therapeutic efficacy must be tailored to evade lysosomal degradation post-endocytosis and allow cytosolic delivery.[22] We loaded RIG-I agonist ppp dsRNA into previously reported LCP NPs.[14] AEAA-conjugated-DSPE-PEG (DSPE-PEG-AEAA) was exploited to facilitate uptake mediated by binding to sigma receptor.[23] Sigma receptors, although their function is not properly understood, are overexpressed in a variety of pancreatic cancer as well as preclinical tumor models.[24] Here, we confirm the expression of sigma receptor in the KPC cell line (Figure S2A). Ligands for the sigma-2 receptor, a subtype of the sigma receptor, had been previously reported to preferentially bind to human and murine pancreatic cancer cell lines, *in vitro* as well as *in vivo*.[25] Our data (Figure S2) suggest that

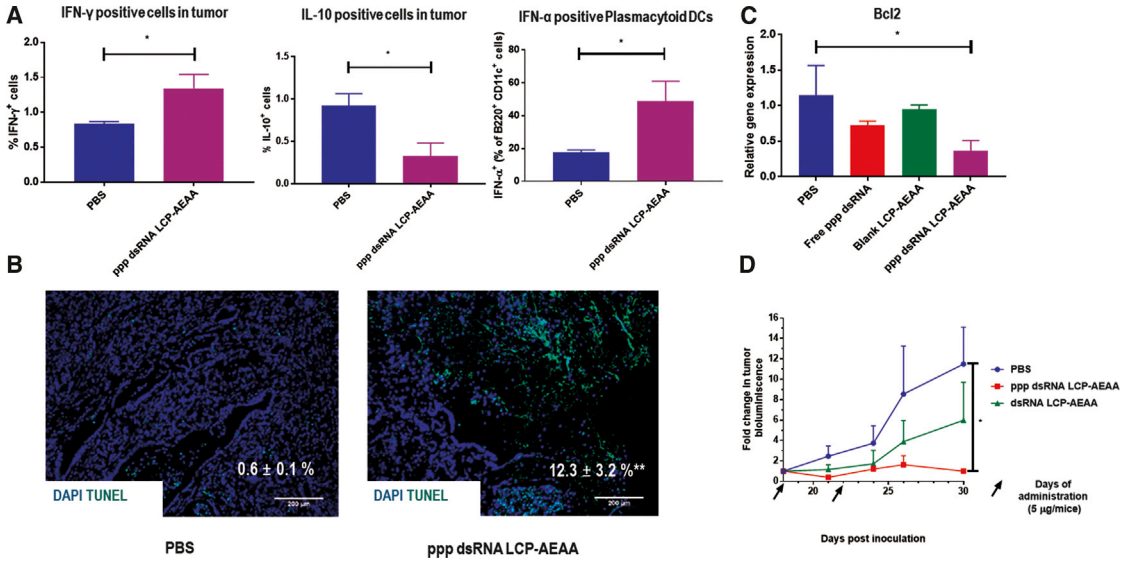

Figure 5. LCP-AEAA Encapsulated with ppp dsRNA Modulates a Proinflammatory Immune Shift and Induces Apoptosis in KPC Tumor by RIG-I Activation and Bcl2 Silencing

(A) After a single treatment of ppp dsRNA LCP-AEAA, KPC-RFP/Luc tumor-bearing mice from intervention groups (n = 3) were randomly sacrificed (18 hr post-administration), stained for cytokines, and analyzed by flow cytometry. (B) Post-treatment as described in Figure 2, KPC-RFP/Luc tumor-bearing mice from intervention groups (n = 3) were randomly sacrificed (day 22). Specimens were stained by terminal deoxynucleotidyl transferase (dUTP) nick end labeling (TUNEL) kit to detect DNA fragmentation. Scale bar, 200 μm. (C) Bcl2 gene expression analysis using qPCR between the treatment groups. (D) Tumor regression study comparing ppp dsRNA LCP-AEAA with both RIG-I activation and Bcl2 siRNA function versus dsRNA LCP-AEAA with only Bcl2 siRNA function (no 5′ triphosphate group). Mice in the PBS group were treated with PBS. Animals received treatments on days 18 and 22 post-inoculation. Data show mean ± SEM (n = 3–4). *$p < 0.05$; **$p < 0.01$.

AEAA targeting can improve the delivery of therapeutic NPs in the pancreatic tumor and further enhance tumor regression.

The biodistribution data revealed that about 2%–3% of the ID distributes to the orthotopic KPC tumor, whereas about 53% of the % ID goes to the liver and 28% goes to the spleen, respectively. High accumulation of NPs in reticuloendothelial system (RES) organs is not atypical and aligns with other recent reports on NP delivery platforms in the orthotopic KPC model.[26] Further, despite a significant accumulation of the adjuvant in the liver, the potential of an inflammatory response is low because the liver is known to be tolerant to PAMPs, being consistently under the exposure to gut-derived flora.[27,28] Interestingly, cellular uptake data (Figure 1B) demonstrated that a higher percentage of fibroblasts take up the particles over cancer cells in the tumor. The fibroblast accumulation is not necessarily a detriment to drug delivery, because fibroblasts are adjacent to tumor cells in pancreatic tumors, and induction of RIG-I by tumor-associated fibroblasts can further potentially augment antitumor signaling by neighboring effect, contrary to an off-targeting-related decrease in therapeutic concentration. In fact, in our previous studies, we managed to harness NP delivery to tumor-associated fibroblasts in an orthotopic xenograft model of pancreatic cancer to produce secretory soluble TNF-related apoptosis-inducing ligand (sTRAIL) triggering apoptosis in adjacent tumor nests.[29]

Previous studies had demonstrated that RIG-I activation by systemic delivery of ppp dsRNA could augment effective antitumor immunity in murine models of pancreatic cancer.[8] Although this stimulates the necessity to further explore PAMP-mediated therapeutic strategies against pancreatic cancer, there are significant toxicological concerns associated with systemic induction of proinflammatory signaling cascade. Further, such studies focused on murine models like Panc02, which lack mutations in relevant genes such as KRAS and tumor protein p53 (TP53) that are involved in driving oncogenesis in an overwhelming majority of human pancreatic cancer patients.[30] KPC is widely recognized as a clinically relevant model of human PDAC in its capacity to manifest the activating oncogenic point mutations KRAS and p53, and to be able to mimic the desmoplastic tumor structure hindering drug delivery.

In this study, KPC tumors underwent significant regression when subjected to two low-dose treatments of ppp dsRNA. Recent studies showed *in vitro* that polyinosinic:polycytidylic acid (poly I:C), a broad-spectrum PAMP interacting with dsRNA-dependent protein kinase (PKR), RIG-I, and melanoma differentiation-associated gene 5 (MDA5), can induce growth arrest in prostate cancer cells for up to about 15 days post-treatment.[31] We demonstrated a similar pattern of tumor growth arrest with the ppp dsRNA encapsulating LCP-AEAAs. Further, with this formulation strategy, we avoided the requirement of repeated administration and could enhance the survival of mice bearing KPC tumor. Thus, we can establish remarkable therapy in a desmoplastic (Figure S3) murine KPC model of PDAC, with a minimal dose (5 μg) of ppp dsRNA, which is about one-tenth of doses reported earlier to induce a robust response.[8,10] We also demonstrated

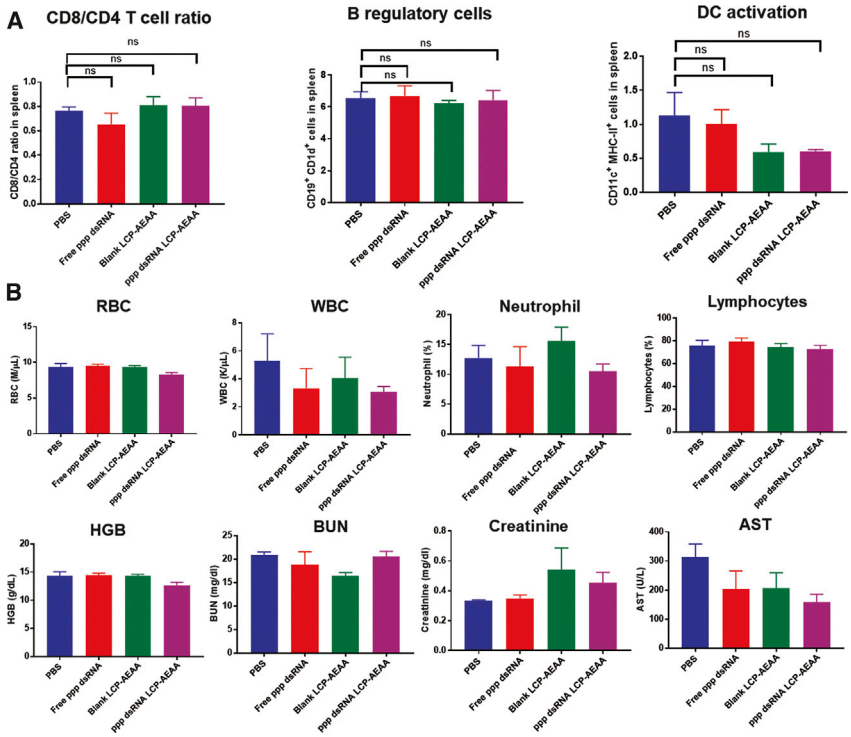

Figure 6. LCP-AEAA Encapsulated with ppp dsRNA Is Non-toxic and Does Not Induce Systemic Immunomodulation

(A) Post-treatment, KPC-RFP/Luc tumor-bearing mice from different intervention groups (n = 3) were randomly sacrificed (day 22). Spleen tissues were harvested, and analysis of different immune cell populations was conducted by flow cytometry. No significant changes were observed in any major lymphocyte population. Key immune cell populations were shown for representation. (B) Biochemistry studies on healthy non-tumor-bearing syngeneic C57BL/6 mice. Animals (n = 5) were administered twice with ppp dsRNA LCP-AEAA/blank LCP-AEAA/free ppp dsRNA/PBS, with an interval of 3 days between subsequent treatments, and sacrificed 3 days after final injection. Blood samples were collected and analyzed to determine changes in RBCs, white blood cells (WBCs), neutrophils, platelets, and lymphocytes. Serum samples were used to analyze liver and kidney function, by measuring changes in blood urea nitrogen, creatinine, and AST. No significant changes were observed. ns, non-significant.

therapeutic efficacy further in a BRAF mutant desmoplastic melanoma model enriched in tolerogenic DC and Treg populations.[32]

RIG-I activation by ppp dsRNA was observed to effectively tune the immunosuppressive cytokine signaling and perturb the tumor infiltrate populations downstream. The T cell infiltrate was enriched in $CD8^+$ T cells, which is correlated with better prognosis in PDAC patients.[33] Systemic depletion of T cells with antibodies against CD8 and CD4 was demonstrated to eliminate the tumor regression benefit as observed with ppp dsRNA LCP. We also observed a strong reduction in TAMs that is associated with poor prognosis in human PDAC patients, most likely because of its role in facilitating the epithelial-to-mesenchymal transition, allowing cancer cell invasion.[34] We further saw an impressive shift in balance toward proinflammatory M1 phenotype. An analogous induction of "classically activated" M1 macrophages under pro-inflammatory signaling had been previously observed in virus-mediated RIG-I activation.[35]

Our study also investigated the role of the Bregs, whose contribution to the oncogenesis of pancreatic cancer is under considerable attention. B cells can cross-talk with T cells and macrophages, programming them toward an immunosuppressive phenotype.[36] The CD1d expression is a shared feature among different subsets of Bregs, and it has been reported that CD1d-producing Bregs can produce immunosuppressive IL-10.[37] $CD138^+$ plasma cells can also express CD1d and are known to mediate immunosuppression by IL-10 and IL-35 production.[38] We found a decrease in the population of both Bregs and immunosuppressive plasma cells in our current study.

We were further interested in the interplay between the tumor-infiltrating cells and the cytokine signaling. Th1 cytokines are known to favor T cell-mediated killing and can further drive cancer cells into senescence.[39] We found an elevation in the levels of the proinflammatory Th1 cytokines and a decrease in the immunosuppressive cytokines like IL-10 and TGF-β. The reduction in the IL-10 levels correlates with our observations of decreasing Breg population in the tumor upon treatment with ppp dsRNA LCP-AEAA. Finally, we investigated the pDC populations that are well characterized to produce type I IFNs upon actuated by PRRs. Although the pDCs have a low expression level of RIG-I-like receptors, they are known to be actuated by RIG-I ligands. However, stimulation by Toll-like receptors (TLRs) is required before an upregulation of RIG-I expression and subsequent sensing of ppp dsRNA may happen.[40] TLRs can be activated by danger-associated molecular patterns (DAMPs) in the tumor microenvironment, so a cross-talk between TLRs and RIG-I-like receptors is not surprising.[41] Additionally, TLR 7 can directly sense dsRNA and trigger IFN-regulatory transcription factor (IRF7) in pDCs.[42] Overall, this indicates a phenotype switch from Th2 to Th1 and a reversal of the suppressive immune microenvironment in the KPC tumor, favorable to promote tumor antigen presentation and induce cytotoxic T cell-mediated killing.

RIG-I helicase activation by ppp dsRNA is immuno-stimulatory by the production of type I IFN. However, it can intrinsically drive apoptosis independent of IFN signaling by activation of Puma and Noxa, BH3-only proteins of the Bcl-2 family that are essential apoptotic regulators.[43] We observed distinct apoptotic regions in the tumor tissue sections when treated with ppp dsRNA LCP-AEAA, which is also an siRNA against anti-apoptotic *Bcl2* by design. However, *Bcl2* silencing alone is not capable of resisting the tumor

progression as effectively as ppp dsRNA, which satisfies the dual objective of RIG-I activation and *Bcl2* silencing.

Although our approach was successful in inducing remarkable immunomodulation and arresting tumor progression, the progression-free survival was not long term, and the tumor eventually escaped growth arrest. Immune homeostasis coupled with proinflammatory RIG-I signaling may limit the efficiency of RIG-I adjuvant therapy and explain the eventual relapse of the tumor progression. Our data have shown a significant increase in IL-6 with ppp dsRNA LCP-AEAA treatment. IL-6 can dampen immunostimulatory activity by JAK/STAT3 signaling to limit the therapeutic efficacy of an RIG-I agonist by negative feedback effect.[44] Our future directions will aim at improving the therapeutic efficacy of our strategy by targeting signaling pathways that drive tolerance to RIG-I signaling and exploiting a tumor antigen capable of driving antigen-specific long-term memory response.

Conclusions

In conclusion, our LCP-AEAA NPs encapsulating ppp dsRNA, an RIG-I agonist and *Bcl2* gene silencing agent, infiltrated the desmoplastic KPC tumor efficiently and provided a robust platform for the local and transient delivery of immunomodulatory RIG-I agonist. The ppp dsRNA LCP-AEAA NPs induced a strong tumor growth inhibition with a significantly lower dose of ppp dsRNA compared with previous reports. Further, the ppp dsRNA treatment allowed progression-free survival and significantly increased overall median survival by 14 days, with only two low-dose treatments. The therapy allowed a reduction in immunosuppressive cell populations and augmented levels of pro-inflammatory Th1 cytokines, suggesting reversal to a proinflammatory tumor microenvironment. We further demonstrated that cells in the tumor could uptake NPs and induce remarkable apoptosis in the orthotopic tumor. Our approach was relatively safe because toxicological analysis did not manifest any noticeable adverse effects. These encouraging results merit further studies of the same approach.

MATERIALS AND METHODS

Materials

DSPE-PEG and 1,2-distearoyl-sn-glycero-3-phosphatidylethanolamine-N-[succinyl(polyethylene glycol)-2000]-N-hydroxysuccinimide (DSPE-PEG2000-N-hydroxysuccinimide [NHS]) were procured from NOF Corporation (Tokyo, Japan). Dioleoyl phosphatidic acid (DOPA) and DOTAP were sourced from Avanti Polar Lipids (Alabaster, AL, USA). Cholesterol was sourced from Sigma-Aldrich (St. Louis, MO, USA). The ppp dsRNA was procured from Invivogen (San Diego, CA, USA) with the strand sequences 5′- pppGCAUGCG ACCUCUGUUUGA-3′ and 3′-CGUACGCUGGAGACAAACU-5′. The control dsRNA without 5′ triphosphate group, with the sequences of the two strands as 5′- GCAUGCGACCUCUGUUUGA-3′ and 3′-CGUACGCUGGAGACAAACU-5′, was also procured from Invivogen. For uptake studies, a custom oligonucleotide with identical strand sequences as the control dsRNA, 5′ labeled with fluorescent Cy5, was procured from Sigma-Aldrich. D-luciferin bioluminescent substrate was purchased from PerkinElmer. All other chemicals were procured from Sigma-Aldrich if not specified otherwise. Six- to eight-week-old female C57BL/6 mice were purchased from Charles River Laboratories (Wilmington, MA, USA). All animal experiments were performed in compliance with and under the approval of the University of North Carolina's (UNC's) Institutional Animal Care and Use Committee.

List of Primers

TaqMan Gene Expression Assays were procured from Thermo Fisher (Waltham, MA, USA) for qPCR. Each assay includes a pair of unlabeled primers and a fluorescent probe with a minor groove binder. The following assays were procured: IL-12α (Mm00434169_m1), IFNγ (Mm01168134_m1), TNF-α (Mm00443258_m1), TGF-β (Mm01178820_m1), IL-6 (Mm00446190_m1), Bcl2 (Mm00477631_m1), and GAPDH (Mm99999915_g1).

List of Antibodies

Brilliant violet 605 anti-mouse CD45, phycoerythrin (PE)/Cy7 anti-mouse CD11c, Pacific Blue anti-mouse F4/80, Alexa Fluor 594 anti-mouse CD8a, allophycocyanin (APC) anti-mouse CD4, fluorescein isothiocyanate (FITC) anti-mouse CD4, peridinin chlorophyll protein complex (PerCP) anti-mouse CD45, PE anti-mouse CD206 (MMR), PE/Cy7 anti-mouse F4/80, APC anti-mouse CD138 (Syndecan-1), FITC anti-mouse CD1d (CD1.1, Ly-38), PerCP anti-mouse CD19, FITC anti-mouse IL-10, FITC anti-mouse I-A/I-E, PerCP/Cy5.5 anti-mouse I-A/I-E, APC/Cy7 anti-mouse CD3, PE anti-mouse/rat/human FOXP3, APC/Cy7 anti-mouse CD86, and APC anti-mouse CD279 (PD-1) were sourced from BioLegend (San Diego, CA, USA). Alpha-Smooth Muscle Actin Monoclonal Antibody (1A4) Alexa Fluor 488, Alpha-Smooth Muscle Actin Monoclonal Antibody (1A4) Alexa Fluor 488, and CD8a Monoclonal Antibody (53-6.7) eFluor 450 were obtained from Thermo Fisher Scientific (Waltham, MA, USA). BD Pharmingen PE Rat Anti-Mouse IFN-γ and BV421 Rat Anti-Mouse F4/80 were procured from BD Biosciences (San Diego, CA, USA). SIGMAR1 (D4J2E) rabbit monoclonal antibody (mAb) was obtained from Cell Signaling Technology (Danvers, MA, USA).

Statistical Analysis

Data were expressed as mean ± SEM, and number of replicates was reported for each experiment (n). GraphPad Prism software was used to execute the statistical analyses using Student's t test, when comparing between two sets of values, and one-way ANOVA when it involved more than three groups, with Tukey's multiple comparisons test for pairwise comparisons. Kaplan-Meier analysis was used for survival study, and significance between treatment groups was determined using log-rank (Mantel-Cox) test. Animals were sorted for *in vivo* experiments by measurement of tumor burden by bioluminescent imaging, ranked in order of average radiance, and drafted into intervention groups. $^{*}p < 0.05$, $^{**}p < 0.01$, $^{***}p < 0.001$, and $^{****}p < 0.0001$, and ns denotes non-significance or $p \geq 0.05$ unless specified otherwise.

Synthesis and Characterization of LCP-AEAA Loaded with ppp dsRNA

LCP NPs were prepared using a protocol as described previously,[19] with additional modifications. In brief, ppp dsRNA (200 μg, 0.25 mg/mL) solution was mixed with $CaCl_2$ (2.5 M, 1,800 μL). An $(NH4)_2HPO_4$ solution (1,800 μL, 50 mM) was independently prepared. The calcium and phosphate solutions were separately added to stirring oil phases prepared with Igepal CO-520 and cyclohexane (3:7 v/v) to drive the formation of calcium phosphate nano-precipitates. The microemulsion was stirred for 5 min before addition of DOPA (20 mM in chloroform or dichloromethane [DCM], 1,400 μL) and stirred further for 30 min. The microemulsion was disrupted by 200 proof ethanol, centrifuged at 10,000 relative centrifugal force (RCF) for 20 min, and further washed with 200 proof ethanol to remove trace Igepal, cyclohexane, and un-encapsulated dsRNA. The precipitate was finally suspended in 10 mL of dichloromethane and centrifuged at 14,000 rpm for 5 min to ensure removal of large aggregates. These "core" NPs were determined to encapsulate approximately 70% of the input ppp dsRNA (14 μg ppp dsRNA/mL DCM). The final particles for therapeutic administration were prepared by adding 357 μL of the "core" LCP, as synthesized in the previous steps to 80 μL of DOTAP (36 mM in DCM), 145 μL of cholesterol (20 mM in DCM), 115 μL of DSPE-PEG (20 mM in DCM), and 13 μL of DSPE-PEG modified with anisamide[45] (DSPE-PEG-AEAA). The lipid film was formed by removal of dichloromethane under nitrogen gas flow, followed by resuspension in 5% glucose solution and sonication before administration. Zeta potential and particle size of LCP were evaluated by a Malvern ZetaSizer (Westborough, MA, USA). 6-Carboxyfluorescein (6-FAM)-modified ppp dsRNA was formulated in LCP, and recovery was evaluated by fluorescence signal intensity.

Biodistribution, Pharmacokinetics, and Cellular Distribution of ppp dsRNA-Loaded LCP-AEAA

For determination of biodistribution and pharmacokinetic profile, ^{177}Lu was used as a radionuclide label. ^{177}Lu was mixed with the $CaCl_2$ phase and formulated into the LCP-AEAA NPs. Mice bearing orthotopic allograft KPC-RFP/Luc tumor (n = 3) were injected with ^{177}Lu-labeled LCPs (25×10^6 counts per minute of ionizing radiation/kg body weight). Blood samples were recovered by tail nick bleed after defined time intervals and detected by gamma scintillation counter. The blood sample data were plotted to determine the percentage of the signal remaining in blood over time. After 24 hr, animals were sacrificed and organs were harvested and washed with PBS, and gamma scintillation was used to determine uptake. $^{177}LuCl_3$ is a beta and gamma emitter. Samples, containers, and waste containing $^{177}LuCl_3$ were handled in accordance with the policies of UNC's Environment, Health and Safety. For determination of LCP-AEAA uptake by different cell populations in the tumor, LCP-AEAA NPs were synthesized with approximately 20% of fluorescent Cy5-labeled dsRNA to form Cy5 oligo-labeled LCP-AEAA, which were injected to mice by intravenous injection (n = 3). 18 hr post-administration, mice were euthanized, and tumors were harvested and processed into single-cell suspensions. Further, cells were stained for fibroblast and tumor-infiltrating lymphocytes by fluorescent-conjugated antibodies, and uptake was quantified by flow cytometry. Here is a representative calculation:

$$\%\ of\ LCP-AEAA\ uptake\ in\ \alpha SMA^{+} cells = \frac{\alpha SMA^{+} Cy5^{+}\ cells}{\alpha SMA^{+}\ \ cells} \times 100\ .$$

Cell Lines

The primary pancreatic tumor cell line derived from the spontaneous KPC model of PDAC (LSL-Kras G12D/+; LSL-Trp53R172H/+; Pdx-1-Cre, of C57BL/6 background) was generously provided by Dr. Serguei Kozlov from the Center for Advanced Preclinical Research, Frederick National Laboratory for Cancer Research (National Cancer Institute [NCI]). Cells were cultured in DMEM:Nutrient Mixture F-12 (DMEM/F12), supplemented with 10% fetal bovine serum (FBS) (GIBCO), 1% penicillin and streptomycin at 37°C and 5% CO_2 in a humidified atmosphere. The primary cell line was transfected with lentiviral vector with mCherry RFP, firefly Luc, and puromycin resistance gene, and selected in the presence of puromycin. The stably transfected cell line (KPC-RFP/Luc) was used for subsequent *in vivo* studies.

Murine BRAF mutant melanoma cell line BPD6 was kindly provided by Dr. Brent Hanks (Duke Cancer Institute, Durham, NC, USA) and grown in RPMI-1640 medium (Invitrogen, Carlsbad, CA, USA) supplemented with 10% FBS (Invitrogen) and 1% penicillin/streptomycin (Invitrogen) at 37°C and 5% CO_2.

Orthotopic Allografting of KPC Model

Sub-confluent KPC-RFP/Luc cells were harvested with 0.05% trypsin-EDTA (GIBCO), washed in PBS, and mixed with an equal volume of Matrigel matrix (Corning). Eight- to ten-week-old C57BL/6 mice were anesthetized by isoflurane inhalation (2%) via a screw fill vaporizer (Matrx Medical). Bupivacaine was administered subcutaneously to the planned site of the incision as a local anesthetic. A midline incision was prepared after abdominal shaving and disinfection; subsequently, spleen and pancreas were gently lifted and 10^6 cells (50 μL) were inoculated into the tail of the pancreas. The skin and abdominal wall were sealed with 6-0 polyglycolic acid sutures. Buprenorphine (Tocris, UK) was administered as a post-operative analgesic.

BLI for Monitoring Tumor Growth

Tumor growth was monitored by Luc imaging using *in vivo* imaging system (IVIS) Lumina Series III (PerkinElmer). Animals were injected with D-luciferin (100 mg/kg of body weight) by intra-peritoneal injection, and images were recorded 10 min post-administration. Bioluminescence signal intensity was reported as average radiance and standardized with respect to average radiance at the initiation of therapy.

Tumor Growth Inhibition and Survival Analysis

Mice bearing KPC-RFP/Luc orthotopic tumors were established as described above. Mice were allocated into four intervention groups (n = 7–10): PBS, free ppp dsRNA, empty LCP-AEAA NPs (blank

LCP-AEAA), and LCP-AEAA NPs encapsulating ppp dsRNA (ppp dsRNA LCP-AEAA), as mentioned in statistical design. Treatments were initiated on day 14. Intravenous injections were performed on days 14 and 18 post-inoculation. Free ppp dsRNA group and ppp dsRNA LCP-AEAA group received 5 μg of ppp dsRNA per injection. Mice were euthanized when average radiance exceeded 10^9 photons/s/cm^2/steradian or demonstrated signs of pain and distress, whichever is earlier.

Subcutaneous Allografting of BPD6 Melanoma Tumor

C57BL/6 mice were inoculated with 1×10^6 BPD6 cells on the lower flank. Once the tumor volume reached approximately 200 mm^3 ($0.5 \times$ length $\times$ width $\times$ height), mice were randomized and sorted into intervention groups (n = 5–8). Treatments were performed on days 13, 15, 17, and 19 post-tumor inoculation, and the doses were maintained consistent to the treatments in the KPC model. Mice were euthanized before tumors attained 20 mm in any one dimension.

Real-Time qPCR Assay

Mice treated with different therapeutics (n = 3) were sacrificed on day 22 post-tumor inoculation, 4 days after second and final treatment. Tumor tissues were harvested and total RNA was extracted using an RNeasy kit (QIAGEN). cDNA was synthesized from RNA with iScript cDNA Synthesis Kit (Bio-Rad). Amplification of cDNA was performed with iQ SYBR Green Supermix system. Mouse-specific primers for qPCRs are procured from TaqMan gene expression assays (Life Technologies). GAPDH was used as an endogenous control. PCRs were conducted with 7500 Real-Time PCR system (Applied Biosystems) and analyzed with the 7500 software.

Flow Cytometry Assay

Spleen and tumor tissues were prepared into single-cell suspensions. In brief, tissues were harvested and enzymatically digested with collagenase A and DNase I at 37°C for 1 hr. The samples were passed through a 70-μm cell strainer. Red blood cells (RBCs) were lysed by addition of ACK buffer, and lysis was quenched by addition of fluorescence-activated cell sorting (FACS) buffer (PBS supplemented with 10% FBS) and centrifuged at 1,400 rpm for 5 min and re-suspended in FACS buffer (5×10^6 cells/mL). Cells were stained with fluorescent-conjugated antibodies, and fluorescence parameters were recorded with Becton Dickinson LSR II (HTS) flow cytometry analyzer. Data were analyzed with FlowJo software platform. FITC Annexin V Apoptosis Detection Kit I (BD Biosciences) was used to stain for Annexin V, according to the manufacturer's instructions.

IF Staining

Major organs and tissues were harvested from animals sacrificed on day 22 post-tumor inoculation, rinsed in PBS, and incubated with 4% paraformaldehyde (PFA) at 4°C for 48 hr. Post-PFA fixation, tissues were washed with water and stored in 70% ethanol solution before being embedded in paraffin. For frozen sections, tissues were harvested, rinsed with PBS, and placed in 4% PFA for 48 hr at 4°C. Following fixation, tissues were placed in 30% sucrose overnight at 4°C for cryoprotection. Tissues were embedded in O.C.T. compound (Fisher Scientific, Pittsburgh, PA, USA) and sectioned by a microtome-cryostat (H/I Hacker Instruments & Industries, Winnsboro, SC, USA). For IF, paraffin-embedded specimens were deparaffinized, and epitope masking was reversed by antigen retrieval and blocked with BSA (1% in PBS). Fluorescent-conjugated antibodies were incubated overnight at 4°C and counterstained with ProLong Gold Antifade mountant (Life Technologies) containing DAPI. Olympus BX61 microscope was used to image samples and analyzed by ImageJ software. TUNEL assays were conducted using the DeadEnd Fluorometric TUNEL System (Promega, Madison, WI, USA) as per manufacturer's instructions. Cell nuclei staining positive for fluorescein-12-dUTP (green) were designated as TUNEL-positive nuclei. Specimens were counterstained with DAPI and analyzed by microscopy as previously described.

Blood Chemistry Analysis

Biochemistry studies were conducted using non-tumor-bearing C57BL/6 mice. In brief, animals were treated with different interventions as described in the Tumor Growth Inhibition and Survival Analysis section, 4 days between subsequent administrations. Four days after final treatment, animals were euthanized, and whole blood and serum samples were collected by cardiac puncture. Complete blood count and clinical chemistry tests to evaluate liver and kidney function were performed with the assistance of Animal Histopathology and Lab Medicine Core at the University of North Carolina at Chapel Hill.

SUPPLEMENTAL INFORMATION

Supplemental Information includes six figures and can be found with this article online at https://doi.org/10.1016/j.ymthe.2018.11.012.

AUTHOR CONTRIBUTIONS

M.D., L.S., Q.L., and L.H. analyzed the data. M.D. and L.H. co-wrote the manuscript. All authors substantially revised the manuscript. M.D., Q.L., L.S., T.J.G., and L.H. helped to conceive and design the *in vivo* experiments. L.H. supervised the project.

CONFLICTS OF INTEREST

The authors declare no competing interests.

ACKNOWLEDGMENTS

The work is supported by NIH grant CA198999 and the Eshelman Institute for Innovation. The UNC Flow Cytometry Core Facility is supported in part by Cancer Center Core Support Grant P30 CA016086 to the UNC Lineberger Comprehensive Cancer Center.

REFERENCES

1. American Cancer Society (2017). Cancer Facts & Figures 2017 (American Cancer Society).
2. Tamburrino, A., Piro, G., Carbone, C., Tortora, G., and Melisi, D. (2013). Mechanisms of resistance to chemotherapeutic and anti-angiogenic drugs as novel targets for pancreatic cancer therapy. Front. Pharmacol. *4*, 56.
3. Bazhin, A.V., Bayry, J., Umansky, V., Werner, J., and Karakhanova, S. (2013). Overcoming immunosuppression as a new immunotherapeutic approach against pancreatic cancer. OncoImmunology *2*, e25736.
4. Ori, D., Murase, M., and Kawai, T. (2017). Cytosolic nucleic acid sensors and innate immune regulation. Int. Rev. Immunol. *36*, 74–88.

5. Lu, C., Xu, H., Ranjith-Kumar, C.T., Brooks, M.T., Hou, T.Y., Hu, F., Herr, A.B., Strong, R.K., Kao, C.C., and Li, P. (2010). The structural basis of 5′ triphosphate double-stranded RNA recognition by RIG-I C-terminal domain. Structure *18*, 1032–1043.
6. Saito, T., and Gale, M., Jr. (2008). Differential recognition of double-stranded RNA by RIG-I-like receptors in antiviral immunity. J. Exp. Med. *205*, 1523–1527.
7. Shekarian, T., Valsesia-Wittmann, S., Brody, J., Michallet, M.C., Depil, S., Caux, C., and Marabelle, A. (2017). Pattern recognition receptors: immune targets to enhance cancer immunotherapy. Ann. Oncol. *28*, 1756–1766.
8. Ellermeier, J., Wei, J., Duewell, P., Hoves, S., Stieg, M.R., Adunka, T., Noerenberg, D., Anders, H.J., Mayr, D., Poeck, H., et al. (2013). Therapeutic efficacy of bifunctional siRNA combining TGF-β1 silencing with RIG-I activation in pancreatic cancer. Cancer Res. *73*, 1709–1720.
9. Knutson, K.L., and Disis, M.L. (2005). Tumor antigen-specific T helper cells in cancer immunity and immunotherapy. Cancer Immunol. Immunother. *54*, 721–728.
10. Poeck, H., Besch, R., Maihoefer, C., Renn, M., Tormo, D., Morskaya, S.S., Kirschnek, S., Gaffal, E., Landsberg, J., Hellmuth, J., et al. (2008). 5′-Triphosphate-siRNA: turning gene silencing and Rig-I activation against melanoma. Nat. Med. *14*, 1256–1263.
11. Akar, U., Chaves-Reyez, A., Barria, M., Tari, A., Sanguino, A., Kondo, Y., Kondo, S., Arun, B., Lopez-Berestein, G., and Ozpolat, B. (2008). Silencing of Bcl-2 expression by small interfering RNA induces autophagic cell death in MCF-7 breast cancer cells. Autophagy *4*, 669–679.
12. Ocker, M., Neureiter, D., Lueders, M., Zopf, S., Ganslmayer, M., Hahn, E.G., Herold, C., and Schuppan, D. (2005). Variants of bcl-2 specific siRNA for silencing antiapoptotic bcl-2 in pancreatic cancer. Gut *54*, 1298–1308.
13. Aznar, M.A., Tinari, N., Rullán, A.J., Sánchez-Paulete, A.R., Rodriguez-Ruiz, M.E., and Melero, I. (2017). Intratumoral delivery of immunotherapy—act locally, think globally. J. Immunol. *198*, 31–39.
14. Satterlee, A.B., and Huang, L. (2016). Current and future theranostic applications of the lipid-calcium-phosphate nanoparticle platform. Theranostics *6*, 918–929.
15. Westphalen, C.B., and Olive, K.P. (2012). Genetically engineered mouse models of pancreatic cancer. Cancer J. *18*, 502–510.
16. Clark, C.E., Beatty, G.L., and Vonderheide, R.H. (2009). Immunosurveillance of pancreatic adenocarcinoma: insights from genetically engineered mouse models of cancer. Cancer Lett. *279*, 1–7.
17. Clark, C.E., Hingorani, S.R., Mick, R., Combs, C., Tuveson, D.A., and Vonderheide, R.H. (2007). Dynamics of the immune reaction to pancreatic cancer from inception to invasion. Cancer Res. *67*, 9518–9527.
18. Goodwin, T.J., Zhou, Y., Musetti, S.N., Liu, R., and Huang, L. (2016). Local and transient gene expression primes the liver to resist cancer metastasis. Sci. Transl. Med. *8*, 364ra153.
19. Liu, Q., Zhu, H., Liu, Y., Musetti, S., and Huang, L. (2018). BRAF peptide vaccine facilitates therapy of murine BRAF-mutant melanoma. Cancer Immunol. Immunother. *67*, 299–310.
20. Swiecki, M., and Colonna, M. (2015). The multifaceted biology of plasmacytoid dendritic cells. Nat. Rev. Immunol. *15*, 471–485.
21. Wang, Y., Zhang, L., Xu, Z., Miao, L., and Huang, L. (2018). mRNA vaccine with antigen-specific checkpoint blockade induces an enhanced immune response against established melanoma. Mol. Ther. *26*, 420–434.
22. Sahay, G., Alakhova, D.Y., and Kabanov, A.V. (2010). Endocytosis of nanomedicines. J. Control. Release *145*, 182–195.
23. Li, S.D., and Huang, L. (2009). Nanoparticles evading the reticuloendothelial system: role of the supported bilayer. Biochim. Biophys. Acta *1788*, 2259–2266.
24. van Waarde, A., Rybczynska, A.A., Ramakrishnan, N.K., Ishiwata, K., Elsinga, P.H., and Dierckx, R.A. (2015). Potential applications for sigma receptor ligands in cancer diagnosis and therapy. Biochim. Biophys. Acta *1848* (10 Pt B), 2703–2714.
25. Kashiwagi, H., McDunn, J.E., Simon, P.O., Jr., Goedegebuure, P.S., Xu, J., Jones, L., Chang, K., Johnston, F., Trinkaus, K., Hotchkiss, R.S., et al. (2007). Selective sigma-2 ligands preferentially bind to pancreatic adenocarcinomas: applications in diagnostic imaging and therapy. Mol. Cancer *6*, 48.
26. Liu, X., Lin, P., Perrett, I., Lin, J., Liao, Y.-P., Chang, C.H., Jiang, J., Wu, N., Donahue, T., Wainberg, Z., et al. (2017). Tumor-penetrating peptide enhances transcytosis of silicasome-based chemotherapy for pancreatic cancer. J. Clin. Invest. *127*, 2007–2018.
27. Boltjes, A., Movita, D., Boonstra, A., and Woltman, A.M. (2014). The role of Kupffer cells in hepatitis B and hepatitis C virus infections. J. Hepatol. *61*, 660–671.
28. Jenne, C.N., and Kubes, P. (2013). Immune surveillance by the liver. Nat. Immunol. *14*, 996–1006.
29. Miao, L., Liu, Q., Lin, C.M., Luo, C., Wang, Y., Liu, L., Yin, W., Hu, S., Kim, W.Y., and Huang, L. (2017). Targeting tumor-associated fibroblasts for therapeutic delivery in desmoplastic tumors. Cancer Res. *77*, 719–731.
30. Wang, Y., Zhang, Y., Yang, J., Ni, X., Liu, S., Li, Z., Hodges, S.E., Fisher, W.E., Brunicardi, F.C., Gibbs, R.A., et al. (2012). Genomic sequencing of key genes in mouse pancreatic cancer cells. Curr. Mol. Med. *12*, 331–341.
31. Langut, Y., Edinger, N., Flashner-Abramson, E., Melamed-Book, N., Lebendiker, M., Levi-Kalisman, Y., Klein, S., and Levitzki, A. (2017). PSMA-homing dsRNA chimeric protein vector kills prostate cancer cells and activates anti-tumor bystander responses. Oncotarget *8*, 24046–24062.
32. Holtzhausen, A., Zhao, F., Evans, K.S., Tsutsui, M., Orabona, C., Tyler, D.S., and Hanks, B.A. (2015). Melanoma-derived Wnt5a promotes local dendritic-cell expression of IDO and immunotolerance: opportunities for pharmacologic enhancement of immunotherapy. Cancer Immunol. Res. *3*, 1082–1095.
33. Carstens, J.L., Correa de Sampaio, P., Yang, D., Barua, S., Wang, H., Rao, A., Allison, J.P., LeBleu, V.S., and Kalluri, R. (2017). Spatial computation of intratumoral T cells correlates with survival of patients with pancreatic cancer. Nat. Commun. *8*, 15095.
34. Liu, C.-Y., Xu, J.-Y., Shi, X.-Y., Huang, W., Ruan, T.-Y., Xie, P., and Ding, J.L. (2013). M2-polarized tumor-associated macrophages promoted epithelial-mesenchymal transition in pancreatic cancer cells, partially through TLR4/IL-10 signaling pathway. Lab. Invest. *93*, 844–854.
35. Shirey, K.A., Pletneva, L.M., Puche, A.C., Keegan, A.D., Prince, G.A., Blanco, J.C., and Vogel, S.N. (2010). Control of RSV-induced lung injury by alternatively activated macrophages is IL-4R alpha-, TLR4-, and IFN-beta-dependent. Mucosal Immunol. *3*, 291–300.
36. Ding, T., Yan, F., Cao, S., and Ren, X. (2015). Regulatory B cell: new member of immunosuppressive cell club. Hum. Immunol. *76*, 615–621.
37. Mauri, C., and Menon, M. (2015). The expanding family of regulatory B cells. Int. Immunol. *27*, 479–486.
38. Shen, P., Roch, T., Lampropoulou, V., O'Connor, R.A., Stervbo, U., Hilgenberg, E., Ries, S., Dang, V.D., Jaimes, Y., Daridon, C., et al. (2014). IL-35-producing B cells are critical regulators of immunity during autoimmune and infectious diseases. Nature *507*, 366–370.
39. Braumüller, H., Wieder, T., Brenner, E., Aßmann, S., Hahn, M., Alkhaled, M., Schilbach, K., Essmann, F., Kneilling, M., Griessinger, C., et al. (2013). T-helper-1-cell cytokines drive cancer into senescence. Nature *494*, 361–365.
40. Szabo, A., Magyarics, Z., Pazmandi, K., Gopcsa, L., Rajnavolgyi, E., and Bacsi, A. (2014). TLR ligands upregulate RIG-I expression in human plasmacytoid dendritic cells in a type I IFN-independent manner. Immunol. Cell Biol. *92*, 671–678.
41. Sato, Y., Goto, Y., Narita, N., and Hoon, D.S. (2009). Cancer cells expressing Toll-like receptors and the tumor microenvironment. Cancer Microenviron. *2* (*Suppl 1*), 205–214.
42. Gantier, M.P., and Williams, B.R. (2007). The response of mammalian cells to double-stranded RNA. Cytokine Growth Factor Rev. *18*, 363–371.
43. Besch, R., Poeck, H., Hohenauer, T., Senft, D., Häcker, G., Berking, C., Hornung, V., Endres, S., Ruzicka, T., Rothenfusser, S., and Hartmann, G. (2009). Proapoptotic signaling induced by RIG-I and MDA-5 results in type I interferon-independent apoptosis in human melanoma cells. J. Clin. Invest. *119*, 2399–2411.
44. Wu, X., Yang, J., Na, T., Zhang, K., Davidoff, A.M., Yuan, B.Z., and Wang, Y. (2017). RIG-I and IL-6 are negative-feedback regulators of STING induced by double-stranded DNA. PLoS ONE *12*, e0182961.
45. Graham, J.P., Authie, P., Karolina Palucka, A., and Zurawski, G. (2017). Targeting interferon-alpha to dendritic cells enhances a $CD8^+$ T cell response to a human CD40-targeted cancer vaccine. Vaccine *35* (35 Pt B), 4532–4539.

YMTHE, Volume *27*

Supplemental Information

Nanoparticle Delivery of RIG-I Agonist Enables Effective and Safe Adjuvant Therapy in Pancreatic Cancer

Manisit Das, Limei Shen, Qi Liu, Tyler J. Goodwin, and Leaf Huang

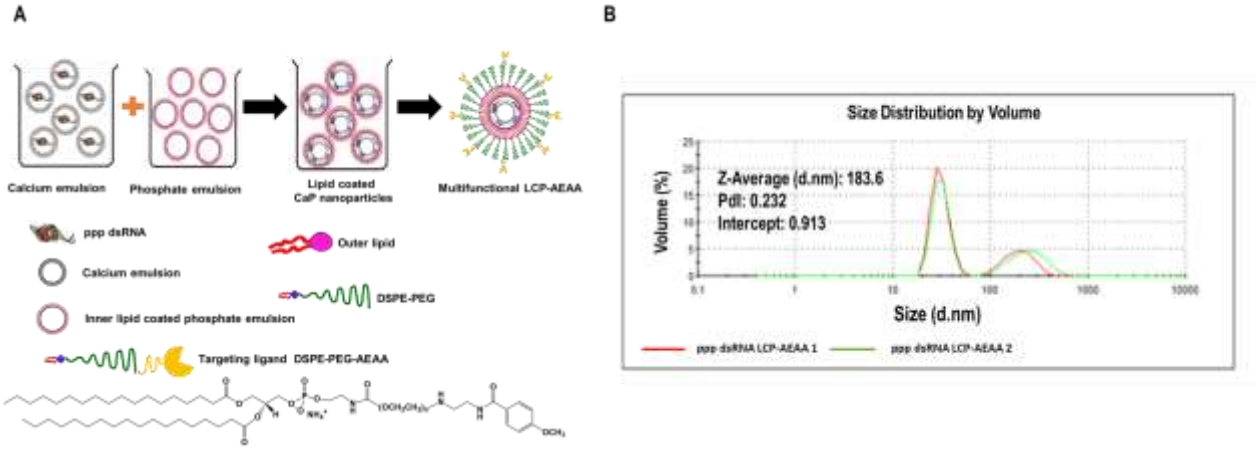

Figure S1: A. Schematic illustration of the LCP-AEAA nanoparticle formulation of ppp dsRNA, B. Size distribution of ppp dsRNA LCP-AEAA by dynamic light scattering. ppp dsRNA LCP-AEAA 1 and ppp dsRNA LCP-AEAA 2 represent two independent batches of the ppp dsRNA LCP-AEAA nanoparticles

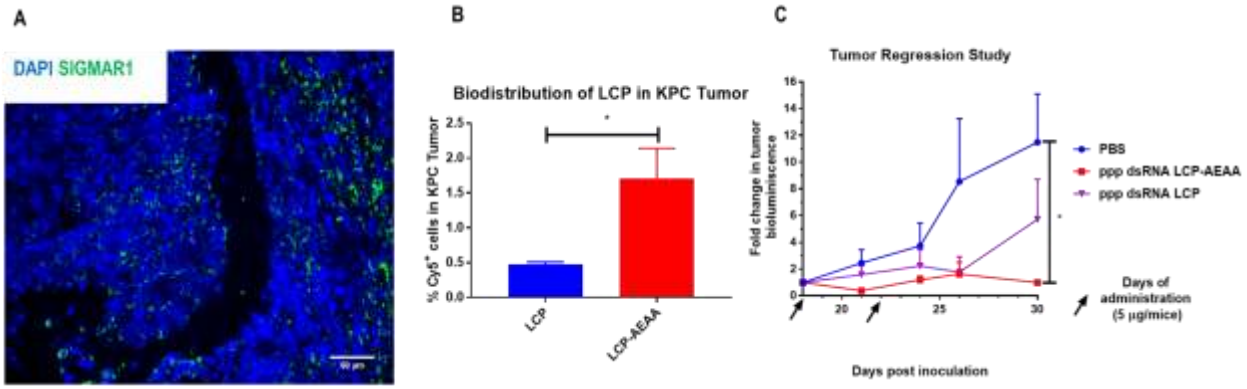

Figure S2. Effect of AEAA targeting on biodistribution & therapy in KPC tumor: A. KPC-RFP/Luc tumors were stained with antibodies against sigma1-receptor (SIGMAR1). Green represents SIGMAR1 and blue represents DAPI respectively, B. KPC-RFP/Luc tumor bearing mice were injected with LCP loaded with Cy5 labeled oligonucleotides. In the untargeted LCP group, DSPE-PEG-AEAA was not incorporated during synthesis of LCPs. Mice were sacrificed after 24 h and percentage of Cy5 positive cells were quantified by FACS (n=3), C. Tumor regression study comparing ppp dsRNA LCP with or without AEAA targeting, as described in Fig. S2B. Mice in PBS group treated with phosphate buffered saline. Animals received treatments on Day 18 and Day 22 post inoculation. Data show mean ± SEM (n = 3-4), *$p < 0.05$

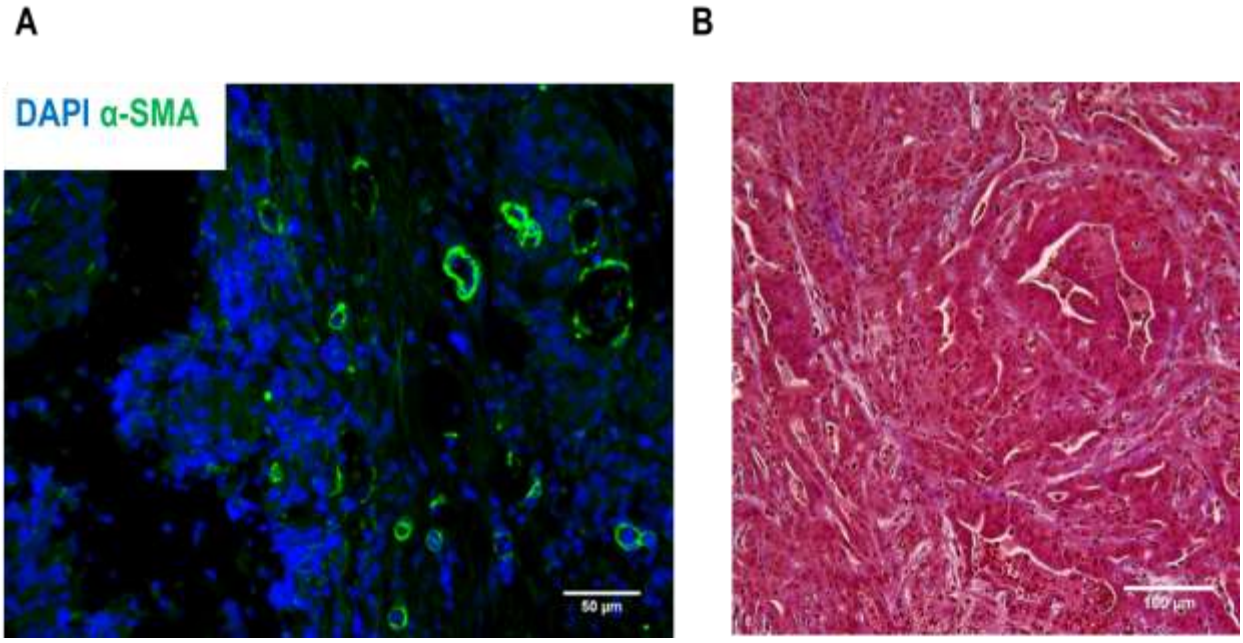

Figure S3: A. KPC-RFP/Luc tumors were stained with antibodies against alpha-smooth muscle actin (α-SMA). Green represents α-SMA and blue represents DAPI respectively. B. Masson's trichrome stain of KPC-RFP/Luc tumor

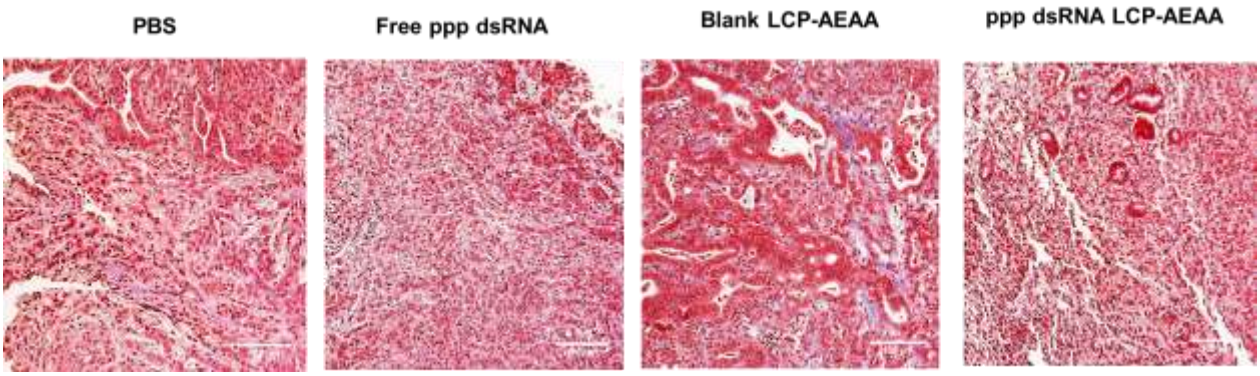

Figure S4: Masson's trichrome stain of orthotopic KPC-RFP/Luc tumor after different treatments

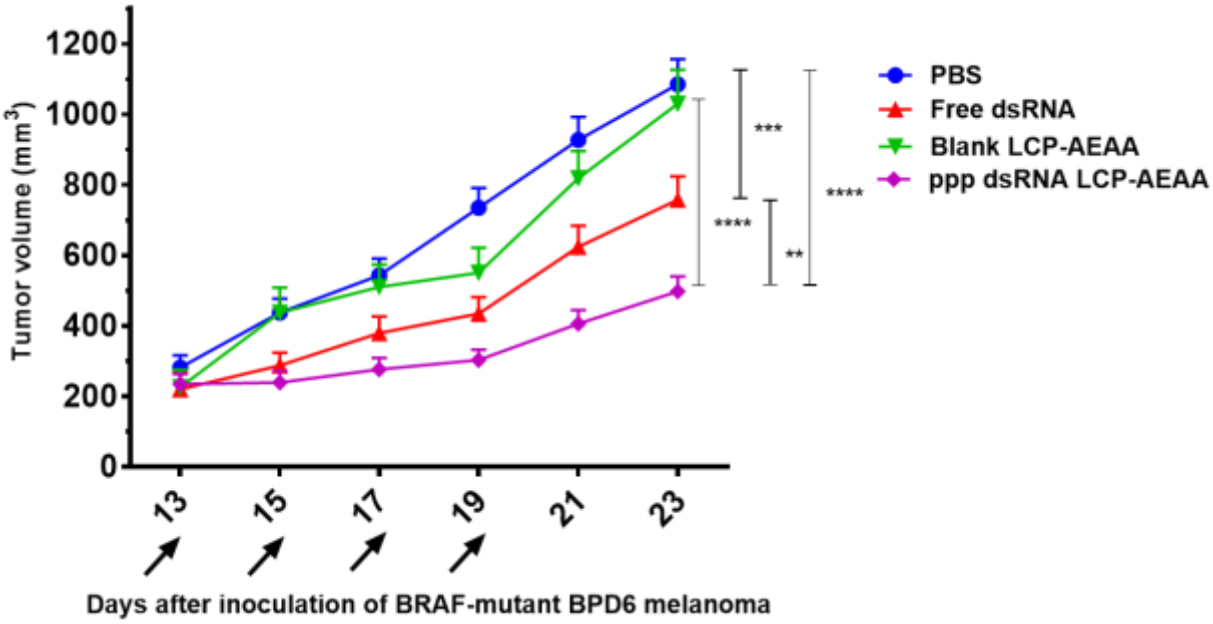

Figure S5: Tumor inhibition curve of subcutaneous syngeneic allograft of murine $BRAF^{V600E}$ PTEN-/- BPD6 melanoma model. Mice were intravenously injected with different therapeutic interventions in same doses as in Fig. 2B. Data show mean ± SEM (n = 4-8), ** $p < 0.01$, ***$p < 0.001$, ****$p < 0.0001$.

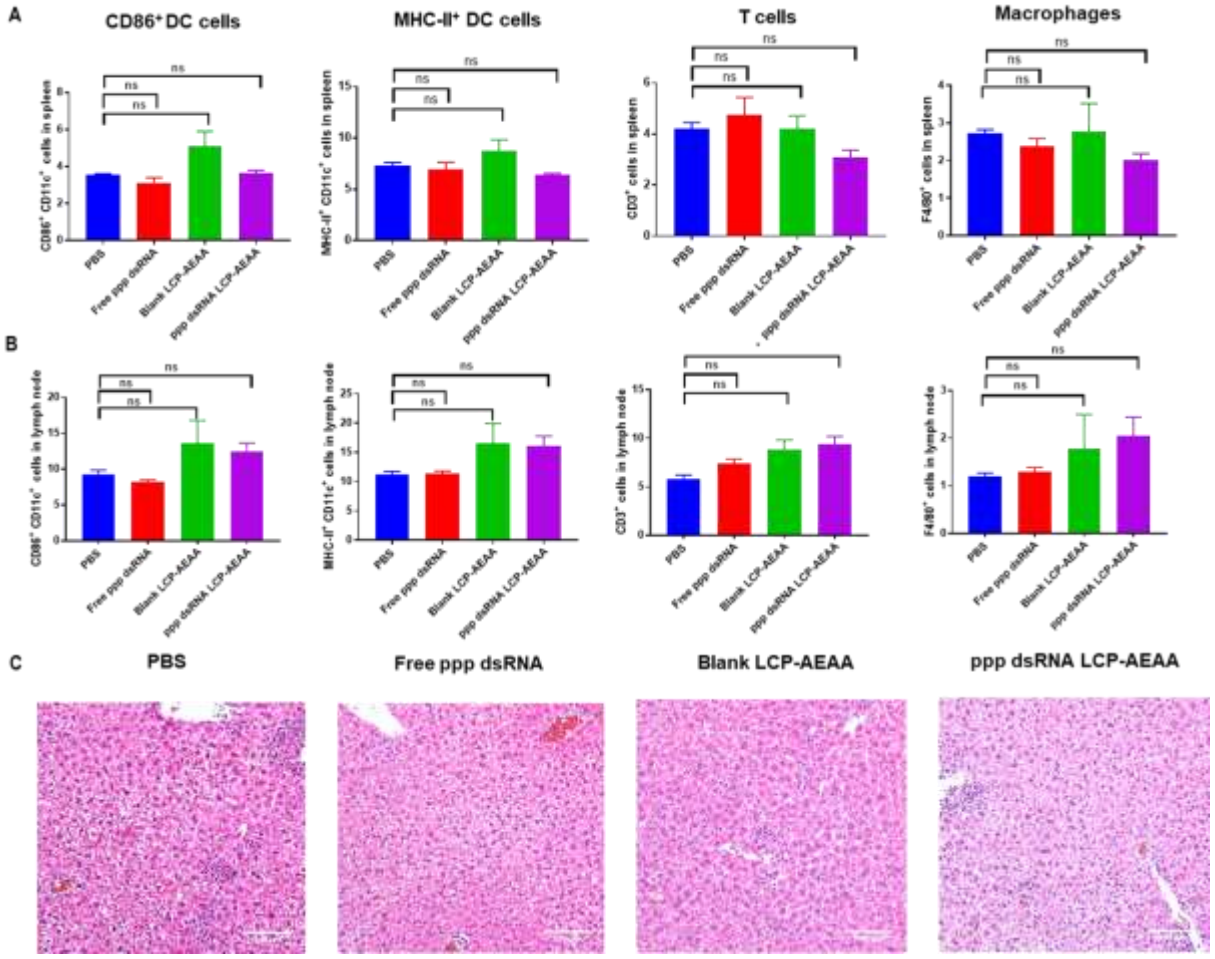

Figure S6: A & B. Healthy non-tumor-bearing syngeneic C57BL/6 mice bearing mice from different intervention groups were sacrificed 16 h post administration. **Spleen** (Fig. S7A) and **lymph nodes** (Fig. S7B.) were harvested and analysis of different immune cell populations was conducted by Flow cytometry. Data show mean ± SEM (n = 4), *p < 0.05, ns denotes non-significant, C. Representative Liver H&E sections from different intervention groups in same study